Journal of Catalysis **195,** 342–351 (2000)
doi:10.1006/jcat.2000.2995, available online at http://www.idealibrary.com on IDEAL®

Influence of the Alkali in Pt/Alkali-β Zeolite on the Pt Characteristics and Catalytic Activity in the Transformation of *n*-Hexane

F. J. Maldonado,* T. Bécue,* J. M. Silva,† M. F. Ribeiro,*,[1] P. Massiani,‡ and M. Kermarec‡

*Departamento de Engenharia Química, Instituto Superior Técnico, Av. Rovisco Pais, 1049-001 Lisboa, Portugal; †Departamento de Engenharia Química, Instituto Superior de Engenharia de Lisboa, Av. Cons. Emídio Navarro, 1949-014 Lisboa, Portugal; and ‡Laboratoire de Réactivité de Surface, Université Pierre et Marie Curie, UMR 7679, CNRS, 4 place Jussieu, 75252 Paris cedex 05, France

Received March 10, 2000; revised June 2, 2000; accepted July 8, 2000

Pt/alkali-β catalysts with various alkali metals (Na, K, Rb, Cs) were prepared by the exchange of alkali-β zeolites with $Pt(NH_3)_4^{2+}$ cations, followed by oxidation and reduction. The reduced Pt particles were characterized and the catalytic activities tested in the transformation of *n*-hexane. The steric constraints, induced by the increase in the size of the alkali, result in a decrease in both the Pt content and the cyclohexane adsorption capacity of the β support. Furthermore, the alkali metal strongly affects the size of the Pt particles and their electronic behavior in the adsorption of CO. Smaller Pt particles are obtained in the presence of the heavier alkali metals, suggesting that the more basic β supports stabilize the Pt species. The Pt dispersion in Pt/Csβ is as high as that in a reference Pt/KL sample prepared under similar conditions. The very small Pt particles in these samples strongly favor aromatization reactions as well as the formation of methylcyclopentane among the C_6 isomers. Moreover, the few cracked products on these samples are related mainly to terminal hydrogenolysis promoted by the metallic sites. In contrast, hydrocracking also takes place on the Pt/Naβ and Pt/KL catalysts owing to their weak acidity. The latter catalysts strongly favor isomerization, independent of the Pt content. Finally, the similar behavior of the Pt/Csβ and Pt/KL zeolites emphasizes the combined roles of the alkali and its porous environment in determining the acid–base properties of the zeolitic support, the stabilization of the Pt species, and the catalytic behavior.

Key Words: β **zeolite; alkali; cesium; basicity; *n*-hexane transformation; platinum.**

INTRODUCTION

Platinum supported on zeolites has been widely studied for the catalytic transformation of paraffins. It is well established that the structure and acid–base properties of the zeolitic support strongly affect the selectivity to the main reactions: the production of light hydrocarbons (hereafter referred to as cracking), isomerization, and dehydrocyclization. The increasing demand for aromatic compounds in the 1980s led to the discovery of the Pt/KL catalyst with exceptional dehydrocyclization behavior (1). Thereafter, oxides and basic zeolites were tested as supports of platinum, and the physicochemistry and catalytic behavior in these systems were reviewed (2, 3). The main hypotheses for explaining the specific behavior of the Pt/KL system are (i) electronic enrichment of the metal particles by interaction with the basic KL support (4–7), (ii) a steric effect related to the channel geometry leading to the concepts of molecular die (8–10) and structural recognition (11), and (iii) the very small size of the platinum clusters (12, 13).

Among all the zeolites tested as supports for platinum, the β zeolite has recently attracted attention. It has been shown that the acidic Pt/Hβ promotes the skeletal isomerization of *n*-hexane (14–16) and that its deactivation during re-forming of methylcyclopentane, ethylcyclopentane, and methylcyclohexane can be minimized by controlling the Brønsted acidity of the β zeolite via dealumination (17). It has also been reported that Pt/Hβ in acid–base composite materials leads to an efficient synergetic effect in re-forming reactions (18, 19). Zheng *et al.* (20, 21) observed that decreasing the acidity of β exchanging the protons for Cs ions enhances the selectivity to benzene during the re-forming of *n*-hexane. They also noted that the Pt/Kβ catalysts are more sulfur resistant than the Pt/KL catalysts (20). Moreover, the use of nonacidic Pt/alkali-β for the catalytic treatment of paraffin feeds has been reported in the patent literature (22).

We recently showed that catalytic stability in the transformation of *n*-heptane of Pt/alkali-β catalysts depends strongly on the nature of the alkali (23). Moreover, we showed that cesium exchanged in β zeolite stabilizes small Pt particles, which are almost as active in the dehydrocyclization of *n*-hexane as the particles in Pt/KL catalysts prepared under similar conditions (24, 25). These previous papers on Pt/alkali-β were focused mainly on the correlation between the physicochemical properties of the catalysts and their ability to produce aromatics. As well as dehydrocyclization, however, other reactions take place such as

[1] To whom correspondence should be addressed. Fax: +351-21-8419062. E-mail: qfilipa@alfa.ist.utl.pt.

0021-9517/00 $35.00

isomerization and cracking, the characteristics of which also depend on the alkali present. This work reports the influence of the nature of the alkali (Na, K, Rb, Cs) in Pt/alkali-β on selectivity to the different reactions that occur during the transformation of *n*-hexane. The detailed analysis of all the products of the reaction gives insight into the nature of the active sites and the mechanisms involved. The catalytic behavior is analyzed in view of the acid–base properties of the zeolitic support and of the Pt particle sizes after reduction. The results are compared to those obtained from a reference Pt/KL sample.

EXPERIMENTAL

(1) Materials

The parent HNaβ zeolite (EXXON, Belgium), was exchanged twice with a 0.5 M $NaNO_3$ solution (70 ml/g, 80°C, 2 h, under stirring). After being washed with water, the solid (zeolite Naβ) was recovered by centrifugation and dried overnight. Zeolites Kβ, Rbβ, and Csβ were obtained by exchanging Naβ for 0.5 M solutions of KNO_3, $RbNO_3$, and $CsCH_3COO$, respectively. The exchange procedures were the same as those mentioned above. The alkali-β zeolites (Naβ, Kβ, Rbβ, and Csβ) were calcined in a flow of air (3 l/h · g) at 500°C for 2 h (heating rate 2°C/min) and then left to rehydrate at ambient atmosphere. The KL zeolite was a commercial sample from UOP (United States).

The calcined alkali-β and KL zeolitic supports were ion-exchanged with $Pt(NH_3)_4^{2+}$ cations by placing 1 g of each sample in contact with 25 ml of a 10^{-3} M aqueous solution of $Pt(NH_3)_4(NO_3)_2$ for 4 h at room temperature with stirring. The expected platinum loading (weight of Pt per weight of zeolite in the suspension) of all the samples was 0.5 wt%. An additional Pt/Naβ sample (called $Pt_{0.25}$/Naβ) was prepared under the same conditions but with a lower Pt loading (0.25 wt% of Pt in the exchange suspension). All the Pt-loaded zeolites were centrifuged, washed with distilled water, and dried for 12 h at 100°C. They were subsequently calcined in a flow of dry air (3 l/h · g) at 300°C for 2 h (heating rate 2°C/min).

(2) Physicochemical Characterizations

The capacity of adsorption of cyclohexane in the alkali-β and KL zeolitic supports was measured at 90°C using a Setaram TG-DSC92 thermobalance. Before adsorption, each sample was pretreated under N_2 (50 ml/min) at 500°C. It was then cooled to 90°C and once the sample weight had stabilized, the N_2 flow was switched to an N_2–cyclohexane flow obtained by bubbling N_2 into a cyclohexane saturator at 14.6°C. The weight increased as a function of time until a maximum value was reached which was taken as the capacity of adsorption.

Pt particle sizes were measured by CO chemisorption and transmission electron microscopy (TEM) after reducing the calcined Pt-loaded zeolites. The reduction before CO chemisorption was carried out *in situ* at 500°C (5°C/min) in H_2 for 2 h followed by evacuation ($<10^{-5}$ mbar) at the same temperature for 2 h. The conditions of chemisorption performed by volumetry at room temperature have been reported in detail (23). The TEM micrographs were obtained on a JEOL 100CXII microscope after reduction of the samples at 500°C under the conditions of the catalytic tests (see below). The average particle size was determined from the size of about 1000 particles.

Pt loading in the reduced samples was obtained by atomic absorption from the Service Central d'Analyse du Centre National de Recherche Scientifique (Vernaison, France).

Transmission FT-IR spectra of CO adsorbed on Pt particles were registered on a Bruker IFS 66 V Fourier transform spectrometer using a resolution of 4 cm^{-1}; 128 scans were accumulated. A self-supported wafer of each calcined Pt-loaded zeolite (ca. 20 mg, 18 mm in diameter, pressed under a pressure of 10^3 kg/cm^{-2}) was put into a quartz holder and placed in an infrared cell equipped with KBr windows and connected to a classical vacuum line. The wafer was reduced *in situ* in a flow of H_2 (5°C/min) at 500°C for 5 h, outgassed ($P < 5 \times 10^{-5}$ mbar) at this temperature for 1 h, and then cooled to room temperature. The background spectrum was that of the sample after reduction. The adsorption of CO was carried out at a pressure of 5×10^{-2} mbar at room temperature. After 15 min, the sample was heated in the closed IR cell at 100°C for 1 h in order to achieve a good distribution of the CO molecules on the metal particles (24, 26) and then outgassed at that temperature for 1 h to minimize dipole–dipole interactions. The FT-IR spectra were registered after the samples were cooled to room temperature.

(3) Catalytic Tests

The *n*-hexane conversion reaction was performed in a flow reactor at 450°C under a total pressure of 1 bar. The calcined Pt-loaded zeolites were reduced *in situ* in a flow of hydrogen (4 l h^{-1} g^{-1}) at 500°C (5°C/min) for 5 h. The reaction feed consisted of a mixture of hydrogen and *n*-hexane (molar ratio $H_2/n\text{-}C_6 = 6$) which was homogenized in a preheated (80°C) vaporizator. The space velocity (WHSV) was 15 h^{-1}, H_2 being used as a carrier gas. The reaction products were separated and identified using an on-line gas chromatograph, equipped with a 100-m plot capillary column (PONA) and a flame ionization detector (FID). The results are reported as conversions (mole percentage of *n*-hexane reacted) and product selectivities (number of moles of product divided by total number of moles formed, in percent).

RESULTS

(1) Physicochemical Characterizations

Except for sample $Pt_{0.25}/Na\beta$, the conditions under which the Pt was introduced into the zeolites were identical. In particular, the Pt content in the suspension was constant, and it was calculated to obtain a Pt loading of 0.5 wt% in all the catalysts, assuming total incorporation of Pt. Despite this, the amount of Pt in the calcined Pt-loaded zeolites varied from one sample to another (Table 1). The exchange of Pt was complete in the $Na\beta$ support, regardless of the Pt content in the platinic suspension (0.25 and 0.5 wt% of Pt). In contrast, only some of the Pt ions were introduced into the other zeolitic supports, the amount of Pt decreasing with increasing size of the alkali cation. Interestingly, this decrease was also related to a decrease in the capacity of the alkali-β support to adsorb cyclohexane (Fig. 1).

The TEM micrographs indicated that the distribution of the Pt particles within the zeolitic crystallites was rather homogeneous except for $Pt/Rb\beta$ in which large Pt particles with diameters above 4 nm are mainly observed; this is associated with a broad distribution of sizes ($1\ nm < d < 12\ nm$). A few large particles ($d > 10$ nm) were also observed at the external surface of the zeolite crystallites of $Pt/Na\beta$ together with the small Pt particles dispersed in the zeolite pores (24).

Table 1 compares the average Pt particle sizes of all samples. For $Pt/Na\beta$, the average particle size was lower when estimated from TEM (2.1 nm) measurements than from CO chemisorption (3.8 nm). In contrast, the average size of the particles in $Pt/K\beta$ and $Pt/Cs\beta$ was larger when determined from TEM measurements than from CO chemisorption; the difference was particularly marked for $Pt/Cs\beta$. These differences will be discussed later. Table 1 shows that the average sizes are similar in $Pt/Cs\beta$ and Pt/KL. Moreover, it indicates that the Pt dispersion in $Pt_{0.25}/Na\beta$ is higher than that in $Pt/Na\beta$ but lower than that in $Pt/Cs\beta$ with similar Pt contents.

TABLE 1

Pt Content, Average Particle Size, and Pt Dispersion in the Pt/Alkali-β and PtKL Catalysts

Catalyst	Pt (wt%)	d^a (nm)	Dispersion[a] (%)	d^b (nm)
$Pt/Na\beta$	0.52	3.8	30	2.1[c]
$Pt_{0.25}/Na\beta$	0.25	1.6	71	N.D.
$Pt/K\beta$	0.38	1.8	64	2.1
$Pt/Rb\beta$	0.33	N.D.	—	4.8
$Pt/Cs\beta$	0.21	1.2	98	1.7
Pt/KL	0.37	N.D.	—	1.7

[a] Average Pt particle size and dispersion of Pt estimated by CO chemisorption.

[b] Average Pt particle size measured by TEM.

[c] In the presence of a few large particles ($4\ nm < d < 18\ nm$); from Ref. (24).

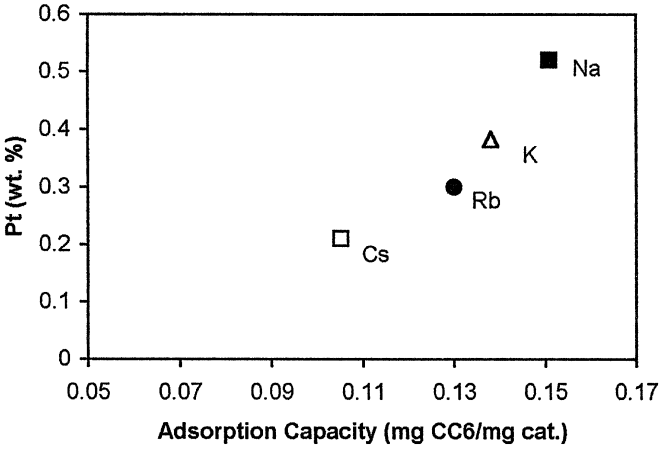

FIG. 1. Amount of platinum in the calcined Pt/alkali-β as a function of the adsorption capacity of cyclohexane of the alkali-β support.

Figure 2 compares the FT-IR spectra of CO adsorbed on the metal particles of Pt/alkali-β and Pt/KL. The intensity of the bands of bridging CO (range 1750–1900 cm^{-1}) in all samples is very low, as usually observed for small Pt particles (26), and the spectra exhibit mainly bands of linear CO (range 1900–2150 cm^{-1}). For $Pt/Na\beta$, a single, smooth peak is shown, centered at 2073 cm^{-1}. This peak is most intense in the spectrum of $Pt/K\beta$, but a shoulder appears in the 2010 to

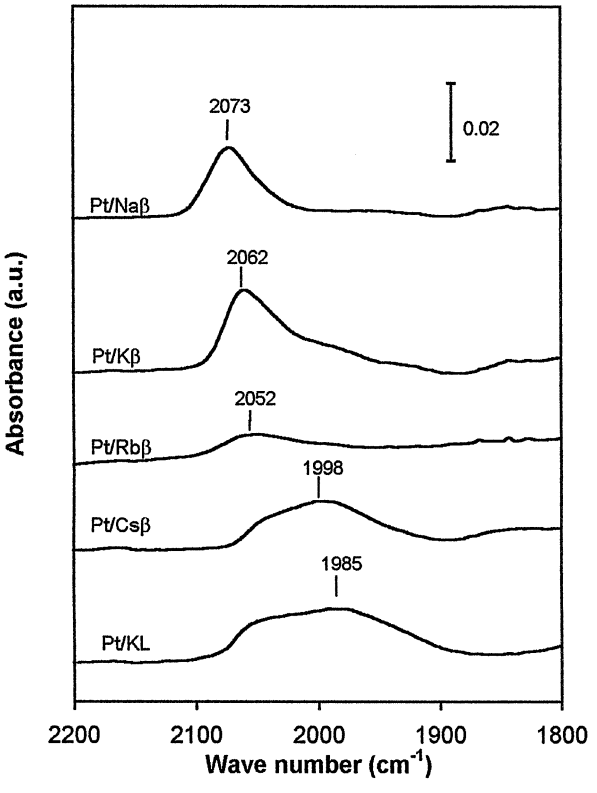

FIG. 2. FT-IR spectra of CO adsorbed on the Pt particles in reduced Pt/alkali-β and Pt/KL.

1980 cm^{-1} range. This shoulder becomes predominant for Pt/Csβ and Pt/KL, the spectra of which exhibit at least two components at low frequency (2045 and 1998 for Pt/Csβ, 2048 and 1985 cm^{-1} for Pt/KL). For Pt/Rbβ, which contains larger (and therefore fewer) Pt particles than those in the above samples (or in other words fewer sites of adsorption of CO molecules), the FT-IR intensity is low, making it difficult to correctly identify the bands.

(2) Catalytic Activity

The catalytic performance of the Pt/alkali-β and Pt/KL catalysts in the transformation of *n*-hexane was evaluated at constant temperature (450°C) and constant space velocity (WHSV = 15 h^{-1}). Figure 3 displays the evolution of conversion with time on stream during the first 3 h of the catalytic runs. The comparison of the curves indicates first that the activity of the catalysts in the series Pt/alkali-β decreases according to the alkali order Na > K > Rb > Cs, the activity of Pt/Naβ being more than twice that of Pt/Csβ. Second, the initial activities are similar for Pt/Naβ and $Pt_{0.25}$/Naβ with the same alkali cation but deactivation is slower in the Pt-richer Pt/Naβ. Third, the activity of Pt/KL is significantly lower than that of Pt/Kβ (same alkali cation but different zeolitic structure), and it is close to that of Pt/Csβ. The deactivation observed for all the catalysts can be attributed to the deposition of coke, its rate depending on the type of cation and on the localization of the Pt particles in the support, as discussed previously (23, 27).

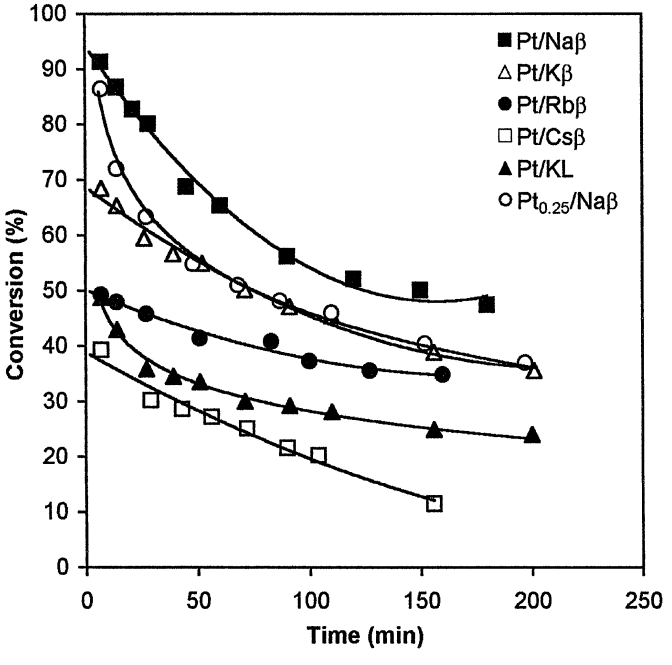

FIG. 3. Evolution of the conversion of *n*-hexane on Pt/alkali-β and Pt/KL catalysts as a function of the reaction time ($T = 450°C$, $H_2/C_6 = 6$, and WHSV = 15 h^{-1}).

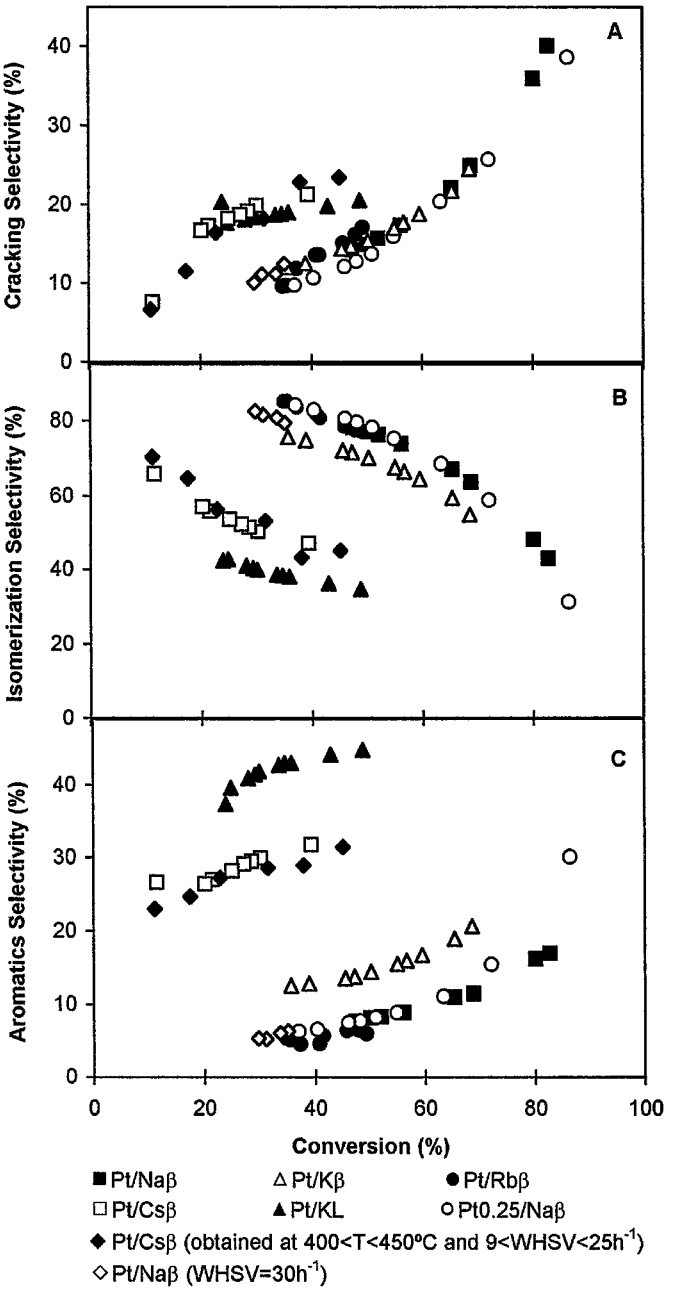

FIG. 4. Selectivity (expressed as mol%) to (A) cracking reactions, (B) isomerization and MCP formation, and (C) aromatization as a function of *n*-hexane conversion for the Pt/alkali-β and Pt/KL catalysts.

(3) Catalytic Selectivity

The analysis of the catalytic selectivity of the Pt/alkali-β and Pt/KL catalysts was performed according to the three main reactions that occur with this type of catalyst: (i) selectivity to cracking (Fig. 4A) assembles all the fragments from C_1 to C_5. (ii) selectivity to isomerization (Fig. 4B) assembles the methylpentanes (MP: 2-MP and 3-MP) and the other C_6 isomers. For the sake of brevity, we decided to include methylcyclopentane (MCP) in the isomerization cut, even though MCP is formed via a C_5 cyclization and,

therefore, contains fewer H atoms than *n*-hexane. This decision was also based on the fact that we discuss the formation of the isomer products over metal centers based on the MCP isomer route that involves C_5 cyclic intermediates. (iii) Selectivity to aromatization (Fig. 4C) is mainly related to benzene formation, but in some cases it includes traces of other aromatics (toluene and xylenes).

The selectivities in Fig. 4 are plotted as functions of the conversion levels which changed because of the deactivation that occurred with time on stream. In order to confirm that the trends in selectivity were not related to the deactivation process, this figure also shows some of the results obtained on Pt/Naβ and Pt/Cs under different catalytic conditions (different WHSV and temperature, see figure caption). Almost no olefins were found.

As for the catalytic activities, the selectivities of Pt/Csβ and Pt/KL were similar with an enhanced formation of aromatics and of light hydrocarbons compared to those of the other Pt/alkali-β samples. In the 35 to 45% conversion range, the selectivity to aromatics reaches 30 to 45% on Pt/Csβ and Pt/KL, whereas it is only 10 to 12% on Pt/Kβ and less than 8% on Pt/Rbβ and Pt/Naβ (Fig. 4C). Similarly, at this conversion level, the selectivity to the C_1–C_5 fragments is higher for both Pt/Csβ and Pt/KL samples than for the other Pt/alkali-β samples (Fig. 4A). In contrast, Pt/Kβ, Pt/Rbβ, and Pt/Naβ strongly favor isomerization (around 80% of C_6 isomers in the 35–45% conversion range, Fig. 4B). In the group of Na, K, and Rb catalysts, it is clear that the curves for Pt/Kβ shift slightly toward those of Pt/Csβ, indicating an intermediate situation.

(4) Product Distribution

The above comparison of selectivity enables us to show the overall trends toward the formation of the three main groups of products. However, a detailed analysis of all the products formed, in particular those present in the light C_1–C_5 hydrocarbons and C_6 isomers, may provide better information about the properties of the catalysts.

Figure 5A compares the percentages of C_1, C_2, C_3, C_4, and C_5 hydrocarbons present in the total C_1 to C_5 fragments at comparable conversions (35–40%) for the various catalysts. The values found for the $Pt_{0.25}$/Naβ catalyst were close to those of Pt/Naβ and are not reported. The most striking result is the predominance of methane in the C_1 to C_5 cut for Pt/Csβ and Pt/KL, whereas C_2 to C_4 products were mainly formed on the other Pt/alkali-β. These trends were also verified for the other conversion levels, as illustrated by the evolution of the $\sum(C_2 - C_5)/C_1$ ratios as a function of the *n*-hexane conversion (Fig. 5B).

The distribution of the C_6 isomers and MCP at similar conversion levels (35–40%) for the various catalysts is shown in Fig. 6A. Skeletal 2MP and 3MP isomers are greater in number over Pt/Naβ, Pt/Kβ, and Pt/Rbβ. In contrast, the proportion of MCP in the C_6 cut is higher on Pt/Csβ and Pt/KL. This tendency is illustrated in Fig. 6B, which plots the MCP/(2MP + 3MP) ratio as a function of the conversion.

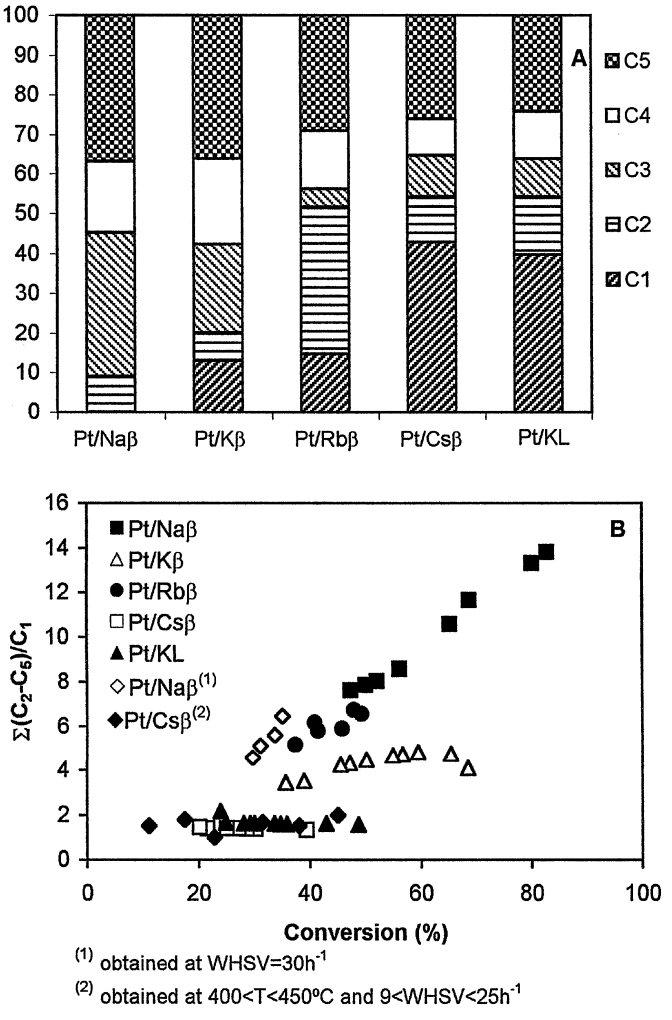

FIG. 5. Distribution of products in the C_1–C_5 fragments formed on the Pt/alkali-β and Pt/KL catalysts: (A) percentages (mol%) of C_1, C_2, C_3, C_4, and C_5 in the total C_1–C_5 cut at conversion levels of about 35 to 40%; (B) ratio $\sum(C_2 - C_5)/C_1$ as a function of the *n*-hexane conversion.

DISCUSSION

The performance of the Pt/alkali-β catalysts in the conversion of *n*-hexane led to a separation of the catalysts into two main groups: on one hand, the Pt/Csβ and Pt/KL catalysts that show aromatization behavior, and, on the other, the Na-, K-, and Rb-containing Pt/β samples, which tend to lead to isomerization. These trends are discussed below in view of the properties of the Pt particles and of the acid–base characteristics of the supports that are modified by changing the alkali cation in the β zeolite.

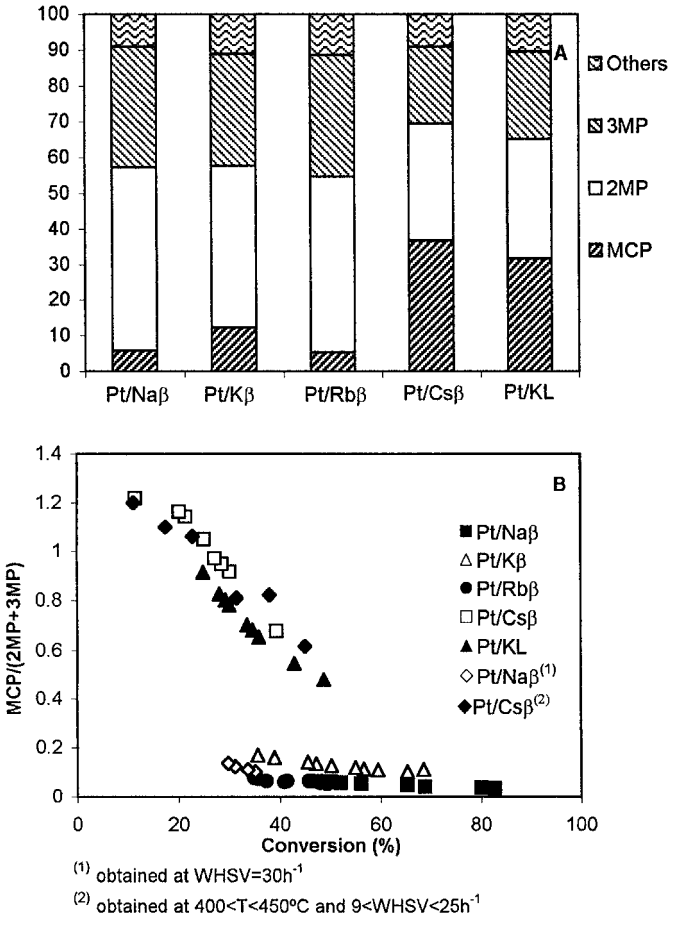

FIG. 6. Distribution of products in the C_6 hydrocarbons cut formed on the Pt/alkali-β and Pt/KL catalysts: (A) percentage (in mol%) of 2MP, 3MP, MCP, and other C_6 isomers in the total C_6 cut at conversion levels of about 35 to 40%; (B) ratio of methylcyclopentane to the sum of methylpentanes (2MP and 3MP) as a function of the *n*-hexane conversion.

(1) Influence of the Alkali on the Characteristics of the Pt Particles

The decreases in both the cyclohexane adsorption capacity of the alkali-β supports and the amount of Pt in the Pt/alkali-β catalysts after changing the alkali indicate that steric constraints occur. The constraints are the lowest in the Naβ support in which all the Pt atoms of the platinic suspension were recovered. It is unlikely that these constraints are related to a partial collapse of the zeolite framework, since the XRD patterns and FT-IR structural bands of all the samples indicate that the samples remained highly crystalline (23). Instead, this decrease suggests an increasing partial blockage of the β porosity when going from the smaller (Na) to the bulkier (Cs) alkali cation. We recently reported that this problem had been overcome by using a slightly different mode of preparation which permitted the introduction of almost all of the Pt atoms in the suspension into the Pt/alkali-β solids, for any alkali (25, 28). Taking into account the low Pt content in Pt/Csβ, we prepared sample $Pt_{0.25}$/Na-β with a similar Pt content to enable us to evaluate the influence of the alkali only.

The discrepancy between the average particle sizes estimated by TEM (2.1 nm) and CO chemisorption (3.8 nm) for the Pt/Naβ sample (Table 1) can be explained by assuming that the large Pt particles (4 nm $< d <$ 18 nm), visible at the external surface of the Naβ crystallites, are more numerous than those actually counted in the micrographs. The larger (and therefore heavier) particles may have decanted from the suspension during preparation of the microtomic cuts and may not have been deposited in the cuts analyzed by TEM, thus leading to an underestimated average size. A similar underestimation may also have occurred in the case of Pt/Rbβ; the hypothesis that Pt was very poorly dispersed is strongly supported by the very low intensity of the FT-IR bands of adsorbed CO. This poor dispersion suggests that something went wrong during the preparation.

In contrast with the above, the average size of the Pt particles in Csβ (and to a lesser extent in Kβ) is smaller when evaluated by CO chemisorption than by TEM. This favors the presence of very small Pt particles with sizes below the limit of detection of the microscope, as already proposed for Pt/Csβ (24) and Pt/KL (2, 3, 12, 13) catalysts. From the above discussion and the data in Table 1, the particle sizes in the various Pt/alkali-β samples can be classified as follows: $d_{Rb} \gg d_{Na} > d_K > d_{Cs}$. In particular, the metal particles in Pt/Csβ are significantly smaller than those in $Pt_{0.25}$/Naβ, despite similar Pt contents. This clearly points out the influence of the nature of the alkali toward particle sizes and the stabilizing effect of the basic Csβ support toward formation of metal nanoparticles. However, the fact that the small Pt particles in Pt/Csβ are similar to those in Pt/KL indicates that not only one (the nature of the alkali) but a combination of parameters (the nature of the alkali associated to the pore structure) are involved in the stabilization of the Pt particles, suggesting that confinement occurs.

The shifts of the FT-IR bands of adsorbed CO from 2073 to 2050 to 1980 cm^{-1}, upon replacing the Na cations by Cs cations in Pt/alkali-β, have been thoroughly discussed and were attributed to changes in the electronic properties associated with changes in the size of the metal particles and the basic properties of the support (24). The similarity of the FT-IR spectra of CO adsorbed in Pt/Kβ and Pt/Naβ indicates that the electronic behavior of the Pt particles is similar in both samples. However, the behavior of Pt in Kβ is somewhat similar to that in Csβ and KL, as revealed by the appearance of the 2040 to 1980 cm^{-1} FT-IR shoulder (Fig. 2). This effect may be related to the Pt dispersion in Pt/Kβ, which is between those in Pt/Naβ and Pt/Csβ (Table 1).

(2) Influence of the Alkali on Catalytic Activity and Stability

The alkali order toward catalytic activity (Na > K > Rb > Cs, Fig. 3) is the same as that of the Pt content in the Pt/alkali-β samples (Table 1). At first glance, this common order seems to suggest that the level of activity is determined by the Pt content. However, many data seem to contradict this hypothesis. Thus, similar initial conversion is obtained on $Pt_{0.25}$/Naβ and Pt/Naβ, in spite of the Pt content which varied by a factor of 2. In this case, however, the lower Pt loading of $Pt_{0.25}$/Naβ was compensated by the higher dispersion (about twice that in Pt/Naβ; Table 1), thereby hardly affecting the conversion, the main effect being only lower catalytic stability (27). A clearer proof that the Pt content is not the determining factor in activity is the much lower conversion obtained on Pt/Csβ than on $Pt_{0.25}$/Naβ with the same Pt contents. This comparison points out a major effect of the nature of the alkali, which modifies not only the accessibility of pores, as shown above, but also the acid–base character of the supports.

The acidity of the Pt/alkali-β catalysts may be generated by protons produced by the reduction of Pt, the presence of defects in the β framework, and the Lewis character of the cations. The acid properties of our samples were analyzed recently (23). On one hand, FT-IR did not reveal acidic OH groups in the Pt/alkali-β catalysts, indicating that the number of protons remained very low, even after reduction. On the other hand, TPD of NH_3 revealed only weak acidity of the Naβ and (but to a lesser extent) Kβ supports, in agreement with the negligible conversions of *n*-hexane obtained on the β supports; the acidity was weak even on the most acidic Naβ support with low conversion of *n*-heptane (about 4%); only the isomerization of butene, used as a model reaction to characterize the acid–base properties, enabled us to differentiate between the acidity of Naβ and Csβ (23). Only traces of acidity were found in Csβ, which is regarded to be a basic material (29). From the above, it is concluded that the samples with the most acidic supports and the lowest diffusionnal constraints are the most active in the transformation of *n*-hexane.

The reasons for the deactivation of the Pt/alkali-β catalysts during the transformation of *n*-heptane and *n*-hexane have already been discussed and analyzed in terms of the formation of coke (favored on the more acidic supports) and the location of the metal particles (23, 27). Deactivation also took place on the present Pt/KL sample, even though Pt/KL is generally considered to be a particularly stable catalyst (1–3). It has been proposed that the high stability of Pt/KL is related to the very small Pt particles located in the intracrystralline pores of the KL zeolite where coke formation is inhibited. Deactivation was then attributed to the presence of larger Pt particles on the external surface of the zeolite crystallites or at the entrance of the pores (30, 31). We assume that such particles were present in our Pt/KL sample, although they were not identified by TEM. We recently prepared a set of more stable Pt/Csβ and Pt/KL catalysts by using another preparation method (25, 28).

(3) Influence of the Alkali on the Catalytic Selectivity

The product selectivities shown in Figs. 4 to 6 reveal that the Cs cation specifically alters the behavior of the β support as compared to the other alkalis. Thus, the selectivity to aromatization in Pt/Csβ approaches that on Pt/KL, whereas isomerization and cracking take place for the most part with the Na-, K-, and Rbβ catalysts. As for the activity, the different Pt contents are not responsible for the different selectivity, since the selectivities of the $Pt_{0.25}$/Naβ and Pt/Naβ samples with the same alkali but different Pt loadings are very similar; they are markedly different for the $Pt_{0.25}$/Naβ and Pt/Csβ samples with comparable Pt loadings but different alkali loadings.

The analysis of the products of the reaction helps to clarify the alkali effect and permits a better understanding of the roles of the acid–base properties, and the characteristics of the Pt particles (size, electron density). Moreover, it enables us to evaluate the mono- or bifunctional character of the catalysts toward the three main reactions.

(a) Analysis of the cracked products. The fragmentation into light hydrocarbons $<C_6$ (or cracking) represents a minor reaction route on all the catalysts (Fig. 4). This reaction can be promoted either by metallic sites (hydrogenolysis) or by acid–metal sites (hydrocracking); the analysis of the product composition in the C_1–C_5 cut may provide information about whether the terminal hydrogenolysis (formation of methane and pentane) or the hydrocracking (formation of C_2, C_3, and C_4) prevails.

Figure 5B shows a plot of the $\sum(C_2 - C_5)/C_1$ ratio, which corresponds to the M_f parameter used in the literature to evaluate the metal or acidic behavior in cracking reactions (32). The M_f values of our catalysts are lower (from 2 to 14) than that (=45) reported for the acidic "Europt-1 + HY" (32), and they are lowest for the Pt/Csβ and Pt/KL samples but were constant over the whole conversion range (Fig. 5B). Both the excess methane and the low M_f value on Pt/Csβ and Pt/KL point to a prevailing terminal hydrogenolysis process on metallic sites and, therefore, a rather monofunctional metallic character. In contrast, the higher M_f value for the other three Pt/alkali-β's suggests a bifunctional character provided by the residual acid sites. The acid site contribution is also proved on Pt/Naβ and Pt/Kβ by the detection of some traces of other aromatics (toluene, ethylbenzene, and xylenes) in the products, beyond benzene, indicating that an additional bifunctional aromatization pathway can take place, as reported previously for Pt/Hβ (14). In the case of Pt/Rbβ with low acidity, the high M_f value is probably due to excess C_2 (Fig. 5A), formed by a multibonding hydrogenolysis process (33) on the large Pt particles.

(b) Analysis of the isomerization products. The isomerization reaction, the favored reaction route in all the catalysts (Fig. 4), can be promoted by metallic or acidic sites. The presence of acid sites should promote the formation of dibranched isomers (dimethylbutanes) (32, 34), such as 2,3-DMB, which were not detected, indicating that the metallic route predominates on all the Pt/alkali-β catalysts. Therefore, although present in some samples, the acidic sites were too weak to promote successive branching. As a result, the C_6 hydrocarbons cut on all the catalysts is composed mainly of MCP, 2MP, and 3MP (Fig. 6A), which are the typical products obtained from the isomerization of *n*-hexane over metallic sites (35). Moreover, the 2MP/3MP ratios measured for all the Pt/alkali-β ($1.4 < 2MP/3MP < 1.7$) agree with the value reported by Christoffel and Páal (2MP/3MP near 2) as being an indicator of the "cyclic" isomerization mechanism on Pt surfaces (36). This mechanism involves surface cyclopentane-like intermediates that may desorb as methylcyclopentane or methylpentanes (37).

The comparison of the MCP/(2MP + 3MP) ratios for the various catalysts (Fig. 6B) emphasizes the higher propensity of Pt/Csβ and Pt/KL to form MCP rather than C_6 isomers as compared to that of the three other catalysts. Considering the following scheme of reactions that occur on metallic sites,

$$n\text{-hexane} \overset{[1]}{\leftrightarrow} \text{MCP} \overset{[2]}{\leftrightarrow} 2\text{MP} + 3\text{MP},$$

it appears that, in the case of Pt/Csβ and Pt/KL, the second step of ring opening is inhibited. For the other three catalysts, reaction [2] proceeds without restrictions, leading to MP isomers.

It has been reported that the ring opening of cyclopentane intermediates to form methylpentanes, which requires the uptake of two hydrogen atoms, is favored in the presence of excess hydrogen (38, 39). Therefore, the ratio of MCP over isomer products can be used as an indicator of the abundance of surface hydrogen under reaction conditions (32). Moreover, it has been proposed that, under reaction conditions at constant H_2 pressure, the availability of hydrogen per surface site of Pt is lower on smaller particles (38). According to these proposals, a higher MCP content in the C_6 product fraction would reveal the presence of smaller Pt particles, which is in line with our results, since the highest MCP/(2MP + 3MP) ratios are obtained on the Pt/Csβ and Pt/KL samples with the smallest Pt particle sizes. Moreover, according to the above-mentioned hypotheses, the increase in the MCP/(2MP + 3MP) ratio observed on the Pt/Csβ and Pt/KL samples with decreasing conversion during the runs (Fig. 6B) is due to a progressive decrease in the amount of surface hydrogen during the deactivation of the Pt particles.

(c) Analysis of aromatization. It is agreed that nonacidic supports are necessary to increase the selectivity to aromatization in the transformation of C_6 and C_7 paraffins (1–3). Moreover, many authors agree on the fact that the small Pt particles are a prerequisite and that the more electron-rich the Pt particles, the higher the benzene selectivity (2, 3).

The specific effect of cesium on the formation of small Pt particles and the high aromatization behavior was discussed in our previous paper on Pt/NaCsβ (24). The average particle size order ($d_{Rb} \gg d_{Na} > d_K > d_{Cs}$) in the present Pt/alkali-β catalysts agrees well with the order of selectivities to aromatization: the smaller the Pt particle, the more selective the catalyst (Fig. 4C). The effect of particle size is particularly clear in the case of Pt/Rbβ in which the large particles have low aromatization properties, despite the basicity of the support, which should be between those of Kβ and Csβ (29). However, as already noted, not only the particle size, but also the basicity of the β support and the proximity of the alkali ions and Pt particles are important (24). A model was recently proposed from atomic XAFS measurements which postulates that the relationships among the catalytic, structural, and electronic properties of small supported Pt particles can all be explained in terms of the metal ionization potential determined by the electrostatic Coulomb interaction between the support and the metal particle (40).

The Pt/Csβ and Pt/KL catalysts with the highest aromatization properties are also those which are the most active for terminal hydrogenolysis (Fig. 5A). A concomitant increase in the properties of aromatization and terminal hydrogenolysis has already been reported (8, 9, 12). Tauster and Steger (8) discussed this effect in terms of the "molecular die concept" and defined the terminal cracking index (TCI) as the C_5/C_4 molar ratio. The selectivity to aromatics, as a function of TCI, presented in Fig. 7 illustrates that

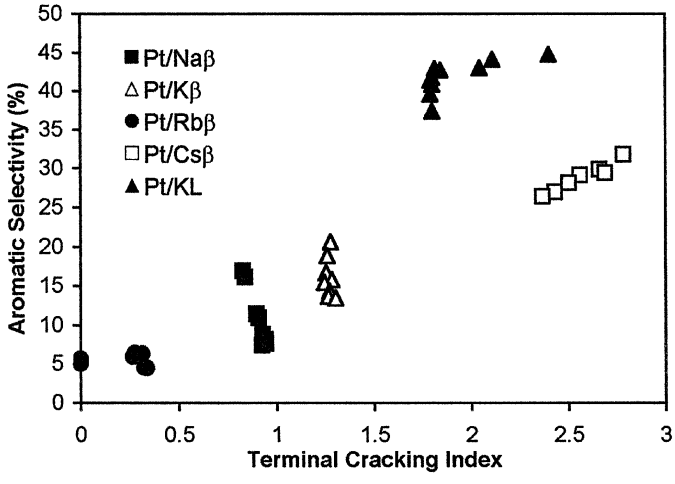

FIG. 7. Evolution of the selectivity to aromatization as a function of the terminal cracking index (TCI) during the runs for the Pt/alkali-β and Pt/KL catalysts.

the TCI is higher for the Pt/Csβ and Pt/KL samples with higher selectivity to benzene, the TCI being >2 in agreement with the literature data (8, 12). In contrast, TCI is <1.5 for the three other Pt/alkali-β catalysts. Moreover, Fig. 7 shows that the greater the Pt particle size (Rb $\gg$ Na > K > Cs), the lower the TCI and the selectivity to aromatization.

The concept of molecular die postulates that the zeolite pore geometry plays a definite role in collimating or preorganizing the paraffin molecules to enable terminal adsorption on the Pt sites (8, 11). Such an effect may take place in the Pt/Csβ catalyst in which diffusional limitation has been proved. However, the hypothesis that space confinement determines aromatization has been challenged in view of the good performance obtained on some nonporous Pt/supports (13, 30), in particular on Pt/Mg(Al)O (13, 41). Other authors proposed that the terminal hydrogenolysis, known as a structure-sensitive reaction on metal surfaces, could be influenced by the geometric effects imposed by the structure of the L zeolite (8). Menacherry and Haller (42) also suggested that the propensity for terminal hydrogenolysis is primarily determined by the morphology of the metal particles and the surface sites exposed to the adsorption of reactants.

Based on a study of the effect of the partial pressure of hydrogen and hydrocarbons, it was proposed that aromatization and hydrogenolysis during the transformation of *n*-hexane are favored under lower hydrogen pressure, whereas more saturated products (i.e., isomers and MCP) are formed in the presence of higher hydrogen pressure (35, 39, 43). Moreover, the prevailing aromatization and hydrogenolysis behavior were explained by the competition between the surface-adsorbed hydrogen and the hydrocarbon molecules. In our study, both the hydrogen and hydrocarbon partial pressures in the gas phase were constant; however, we postulated above that the hydrogen concentration on the surface of the Pt particles depends on the particle size of Pt. Taking into account the different particle size of Pt in the Pt/alkali-β, the role of the concentration of surface hydrogen, and the hydrogen sensitivity of the different reactions, it is possible to explain the differences in the hydrogenolysis behavior. Thus, the lower hydrogen availability on the smallest particles of Pt/Cs-β and Pt/KL would make these particles more accessible for the adsorption of neighboring C–C, thus leading to higher hydrogenolysis. This hypothesis is supported by the presence of very small particles in both catalysts, and showing the tendency of these nanoparticles to promote aromatization and hydrogenolysis. However, the small particles in $Pt_{0.25}$/Naβ promote neither hydrogenolysis nor aromatization, suggesting again that not only the particle size, but also factors such as the acidobasicity, the space confinement, and the proximity of the alkali and Pt particles, may play a determining role in catalytic behavior.

CONCLUSION

The nature of the alkali in Pt/alkali-β zeolites strongly affects the acid–base properties of the β support and the characteristics of the Pt particles. In turn, it considerably alters the catalytic activity in the transformation of *n*-hexane and the selectivity toward the three main reactions, i.e., cracking, isomerization, and aromatization.

The most acidic samples (Na > K > Rb > Cs) are the most active, independent of the Pt content. Acidity promotes the hydrocracking reactions, giving high proportions of C_2, C_3, and C_4 hydrocarbons in the C_1–C_5 cut (samples Pt/Naβ and Pt/Kβ). Cracking also takes place on nonacidic Pt/Csβ, but is related rather to terminal hydrogenolysis on the metallic sites, giving large amounts of methane. However, not only the acidity of the supports but also the size of the Pt particles must be considered when explaining the distribution of the cracked products, since a multibonding hydrogenolysis process can occur when large Pt particles are present as was shown for the Pt/Rbβ sample on which a high proportion of C_2 was formed. For the isomerization reaction, a metallic monofunctional mechanism prevails, for any alkali, which is in line with the absence of strong acidic sites.

The proposal that aromatization during the transformation of *n*-hexane requires the presence of very small Pt particles is fully supported by our results. Indeed, the catalysts could be divided into two main groups: the catalysts with an average Pt particle size above 1.6 to 2.0 nm, promoting isomerization (samples Pt/Naβ, Pt/Kβ, and Pt/Rbβ), and catalysts with smaller Pt particles, promoting aromatization (samples Pt/Csβ and Pt/KL). Moreover, our results confirm that those catalysts that are the most selective to aromatization are also those in which terminal hydrogenolysis and the formation of methylcylopentane (among C_6 isomers) are favored, which may be related to a smaller amount of available surface hydrogen on Pt with a smaller particle size.

Finally, the increase in the Pt dispersion in the Pt/alkali-β samples when the alkali is changed from Na to K and then to Cs emphasizes the role of the alkali (or in other words that of the acid–base properties of the support) on stabilization of the Pt particles. However, not only the alkali but also its porous environment play a determining role, since similar small particles are obtained in Pt/Csβ and Pt/KL zeolites, suggesting that confinement effects are involved.

ACKNOWLEDGMENTS

We acknowledge support of this work by the European Commission (HCM network contract ERBCHRXCT 940477), and the CNRS-ICCTI (project no. 7043). The authors thank M. Lavergne for conducting the TEM experiments.

REFERENCES

1. Bernard, J. R., *in* "Proc. 5th Int. Zeol. Conf., Naples" (L. V. C. Rees, Ed.), p. 686. Heyden, London, 1980.
2. Davis, R. J., *Heterog. Chem. Rev.* **1**, 41 (1994).
3. Meriaudeau, P., and Naccache, C., *Catal. Rev. Sci. Eng.* **39**, 5 (1997).
4. Besoukhanova, C., Breysse, M., Bernard, J. R., and Barthomeuf, D., *Stud. Surf. Sci. Catal.* **6**, 201 (1980).
5. Besoukhanova, C., Guidot, J., Barthomeuf, D., Breysse, M., and Bernard, J. R., *J. Chem. Soc., Faraday Trans. 1* **77**, 1595 (1981).
6. Larsen, G., and Haller, G. L., *Catal. Lett.* **3**, 103 (1989).
7. Dong, J. L., Zhu, J. H., and Xu, Q. H., *Appl. Catal. A: Gen.* **112**, 105 (1994).
8. Tauster, S. J., and Steger, J. J., *J. Catal.* **125**, 387 (1990).
9. Lane, G. S., Modica, F. S., and Miller, J. T., *J. Catal.* **129**, 145 (1991).
10. Gao, Z., Jiang, X., Ruan, Z., and Xu, Y., *Catal. Lett.* **19**, 81 (1993).
11. Derouane, E. G., and Vanderveken, D. J., *Appl. Catal.* **45**, L15 (1988).
12. Mielczarski, E., Hong, S. B., Davis, R. J., and Davis, M. E., *J. Catal.* **134**, 359 (1992).
13. Davis, R. J., and Derouane, E. G., *Nature* **349**, 313 (1991).
14. Smirniotis, P. G., and Ruckenstein, E., *J. Catal.* **140**, 526 (1993).
15. Lee, J.-K., and Rhee, H.-K., *Catal. Today* **38**, 235 (1997).
16. Leu, L. J., Hou, L. Y., Kang, B. C., Li, C., Wu, S. T., and Wu, J. C., *Appl. Catal.* **69**, 49 (1991).
17. Smirniotis, P. G., and Ruckenstein, E., *Appl. Catal. A: Gen.* **117**, 75 (1994) and *Catal. Lett.* **25**, 351 (1994).
18. Ruckenstein, E., and Smirniotis, P. G., *Catal. Lett.* **24**, 123 (1994).
19. Smirniotis, P., and Ruckenstein, E., *Appl. Catal. A: Gen.* **123**, 59 (1995).
20. Zheng, J., Dong, J. L., and Xu, Q. H., *Stud. Surf. Sci. Catal.* **84**, 1641 (1994).
21. Zheng, J., Dong, J. L., Xu, Q. H., Liu, Y., and Yan, A. Z., *Appl. Catal.* **126**, 141 (1995).
22. Dessau, R., U.S. Patent 4,929,792 (1990) and U.S. Patent 5,011,805 (1991).
23. Maldonado-Hodar, F. J., Ribeiro, M. F., Silva, J. M., Antunes, A. P., and Ribeiro, F. R., *J. Catal.* **178**, 1 (1998).
24. Becue, T., Maldonado, F. J., Antunes, A. P., Silva, J. M., Ribeiro, M. F., Massiani, P., and Kermarec, M., *J. Catal.* **181**, 244 (1999).
25. Jia, C., Antunes, A. P., Silva, J. M., Ribeiro, M. F., Lavergne, M., Kermarec, M., and Massiani, P., *Stud. Surf. Sci. Catal.* **130**, 2993 (2000).
26. Sheppard, N. J., and Nguyen, T. T., *Adv. Infrared Raman Spectrosc.* **5**, 67 (1978).
27. Maldonado-Hodar, F. J., Silva, J. M., Ribeiro, F. R., and Ribeiro, M. F., *Catal. Lett.* **48**, 69 (1997).
28. Taibi, M., *et al.*, to be published.
29. Barthomeuf, D., *Catal. Rev.* **38**, 521 (1996).
30. Iglésia, E., and Baumgartner, J. E., *in* "Proceedings, 9th International Zeolite Conference" (R. Von Ballmoos, J. B. Higgins, and M. M. J. Treacy, Eds.), Vol. II, p. 421. Butterworth-Heinemann, London, 1992.
31. Jentoft, R. E., Tsapatsis, M., Davis, M. E., and Gates, B. C., *J. Catal.* **179**, 565 (1998).
32. Paál, Z., Zhan, Z., Manninger, I., and Sachtler, W. M. H., *J. Catal.* **155**, 43 (1995).
33. Frennet, A., *in* "Hydrogen Effects in Catalysis: Fundamentals and Practical Applications" (Z. Paál and P. G. Menon, Eds.), Vol. 31, p. 399. Dekker, New York, 1988.
34. Allain, J. F., Magnoux, P., Schulz, Ph., and Guinest, M., *Appl. Catal. A: Gen.* **152**, 221 (1997).
35. Paál, Z., *Adv. Catal.* **29**, 273 (1980).
36. Christoffel, E., and Paál, Z., *J. Catal.* **73**, 30 (1982).
37. Barron, Y., Maire, G., Muller, J. M., and Gault, F. G., *J. Catal.* **5**, 428 (1966).
38. Paál, Z., *Catal. Today* **12**, 297 (1992).
39. Paál, Z., *in* "Hydrogen Effects in Catalysis: Fundamentals and Practical Applications" (Z. Paál and P. G. Menon, Eds.), Vol. 31, p. 449. Dekker, New York, 1988.
40. Mojet, B. L., Miller, J. T., Ramaker, D. E., and Koningsberger, D. C., *J. Catal.* **186**, 373 (1999).
41. Davis, R. J., and Derouane, E. G., *J. Catal.* **132**, 269 (1991).
42. Menacherry, P. V., and Haller, G. L., *J. Catal.* **177**, 175 (1998).
43. Paál, Z., Groeneweg, H., and Zimmer, H., *Catal. Today* **5**, 199 (1989).